LYAPUNOV ORBITS IN THE JUPITER SYSTEM USING ELECTRODYNAMIC TETHERS

Kevin Bokelmann[*], Ryan P. Russell[†], and Gregory Lantoine[‡]

Various researchers have proposed the use of electrodynamic tethers for power generation and capture from interplanetary transfers. The effect of tether forces on periodic orbits in Jupiter-satellite systems are investigated. A perturbation force is added to the restricted three-body problem model and a series of simplifications allows development of a conservative system that retains the Jacobi integral. Expressions are developed to find modified locations of equilibrium positions. Modified families of Lyapunov orbits are generated as functions of tether size and Jacobi integral. Zero velocity curves and stability analyses are used to evaluate the dynamical properties of tether-modified orbits.

INTRODUCTION

There is increasing interest in missions to the outer planets, highlighted by the most recent decadal survey. Among many unique challenges of outer planet missions, extreme distances from the Sun lead to restrictive power constraints. In particular the large Sun-spacecraft distances limit the use of solar cells due to solar radiation decreasing as an inverse square law. While the ongoing Juno mission to Jupiter is able to make use of solar cells its power is less than 500 W, limiting its science capabilities.[1] The common alternative to solar power is using radioisotope thermal generators (RTGs) such as those used for Cassini and Galileo. These come with their own set of problems, including political and safety issues that arise when dealing with radioactive materials.

A developing alternative is making use of the rotating magnetic field of planets through electrodynamic tethers. Jupiter is of greatest interest due its strong magnetic field but magnetic fields exist at the Earth and the other gas giants as well. The premise of using a tether to provide power relies on basic principles of electromagnetism, namely that current is induced when a conductor moves through a magnetic field. This current generation makes for an attractive alternative power source for spacecraft, replacing solar cells that become increasingly ineffective far from the Sun, or radioisotope thermal generators that are complex and in limited supply.[2,3] Power scarcity is a common limiting factor in spacecraft design so this additional source is of much practical interest. Research has explored power generation in different motion regimes including during system satellite tours as well as orbiters stationary relative to a secondary body.[4,5,6]

The second capability of electrodynamic tethers is as a force generator. Charged particles (such as current in a tether) moving through a magnetic field create what is known as the Lorentz force. This force is a function of position, velocity, and tether orientation and is non-conservative. Given that this force can be generated with negligible propellant used for attitude control there is potential for significant mass savings. The largest potential for propellant mass reduction comes from applications to departure and capture for interplanetary trajectories as these are typically large fractions of propellant budgets. Initial and ongoing research shows that capture from hyperbolic orbits can be greatly assisted if not completely performed by electrodynamic tethers.[7,8,9] Other work shows how tethers can be used for orbital transfers about a single body.[10] Also of interest is the efficiency of tethers for these transfers in terms of mass

[*] Graduate Student, Aerospace and Engineering Mechanics, The University of Texas at Austin, kbokelmann@utexas.edu.
[†] Assistant Professor, Aerospace and Engineering Mechanics, The University of Texas at Austin, 1 University Station, C0600 Austin, TX 78712-0235, ryan.russell@utexas.edu.
[‡]

relative to electrical thrusters where it has been shown that tether systems can be lighter over long-term applications.[11]

An application of the Lorentz force is that it alters the equilibrium points in the circular restricted three-body problem (CRTBP). Research has been done on the stability and dynamics for tethers operating at these modified equilibrium points, typically in the interest of power generation without deorbiting. Various analyses have shown that these equilibrium points are stable or can be made stable through the use of control laws.[12,13,14,15] The next step is to expand these equilibrium points into fully periodic orbits in the three-body system. In the typical three-body model these periodic orbits are being considered for a variety of applications including parking orbits, inter-moon transfers, and as descope alternatives to science orbits.[16,17,18] The addition of a tether can makes spacecraft self-powered but introduces Lorentz forces that will alter the orbits. Knowledge of the effect of these forces on orbit orientation and stability is needed for a full end-to-end mission design with tethers.

PROBLEM DEFINITION

The CRTBP is used to model the gravitational dynamics of the spacecraft influenced by Jupiter and one of its moons. Although the focus is on planar motion, the full model is used to study the planar stability to out-of-plane perturbations. Unlike other works such as References 12 and 15, the Hills approximation is not considered as variations in the magnetic field strength prevent a general scaling applicable to all moons, eliminating one of the main benefits of using the Hill model. Using a rotating frame centered at the system center of mass the equations of motion are described by Equation (1)

$$\ddot{\mathbf{r}} + 2\boldsymbol{\Omega} \times \dot{\mathbf{r}} = \nabla \mathbf{J} \tag{1}$$

where the spacecraft center of mass position is given by $\mathbf{r} = (x, y, z)$, velocity is $\dot{\mathbf{r}} = (u, v, w)$, and the frame rotates with the primaries at angular rate . The potential-like function J is given in Equation (2):

$$J = \frac{1}{2} \quad {}^{2}(x^2 + y^2) + \frac{1-\mu}{r_1} + \frac{\mu}{r_2} \tag{2}$$

where r_1 and r_2 are the distances of the spacecraft from the respective primaries and μ is the ratio of the smaller primary gravitational parameter to the sum of both primary's gravitational parameters. Normalization factors are used to convert to dimensionless units such that the distance between the primaries is one length unit (LU) and the frame rotation is one radian per time unit (TU).

The tether dynamics are treated as a perturbing force to the circular restricted three-body model dynamics giving Equation (3):

$$\ddot{\mathbf{r}}_{\mathbf{EDT}} + 2\boldsymbol{\Omega} \times \dot{\mathbf{r}} = \nabla \mathbf{J} + k\mathbf{f}_{\mathbf{L}} \tag{3}$$

where k is a normalizing constant that converts the force to dimensionless acceleration. Assuming the force is given in newtons and LU is expressed in kilometers:

$$k = \frac{TU^2}{1000LU \cdot m_{sc}} \tag{4}$$

where m_{sc} is the spacecraft mass. As stated previously, the tether works on the electrodynamic principle of the Lorentz force where a conductive wire moving in a magnetic field has an induced current which reacts with the magnetic field to cause a force. The induced electric field is dependent on the inertial relative velocity between the spacecraft and the plasma fixed to Jupiter's magnetic field:

$$\mathbf{E} = (\mathbf{v_{sc}} - \mathbf{v_{pl}}) \times \mathbf{B}(\mathbf{r}) \tag{5}$$

$$\mathbf{v_{pl}} = \boldsymbol{\omega}_\mathbf{J} \times \mathbf{r_1} \tag{6}$$

where **B** is the local vector of the magnetic field and $\boldsymbol{\omega}_\mathbf{J}$ is the rotation vector of Jupiter. Using a bare tether with length L and width w, averaging the current along the length of the tether, and choosing the zero-bias point for maximum current gives the Lorentz force in newtons[13]:

$$I_{avg} = \frac{3}{5} I_0 \tag{7}$$

$$I_0 = \frac{4}{3}\left(\frac{w}{\pi}\right) q_e N_e L^{3/2} \sqrt{2E_t(q_e/m_e)} \tag{8}$$

$$\mathbf{f_L} = I_{avg} L(\hat{\mathbf{u}} \times \mathbf{B}) \tag{9}$$

The current depends on the orientation of the tether with the electric field as $E_t = \mathbf{E} \cdot \hat{\mathbf{u}}$, where the tether direction $\hat{\mathbf{u}}$ is measured aligned with the tether and points towards the tether cathode. Magnetic field properties are included where q_e and m_e are the charge and mass of an electron and N_e is the local plasma electron density. The actual magnetic field of Jupiter is off-set from Jupiter center and tilted by 10.77° from the Jupiter rotational plane, resulting in non-autonomous dynamics.[19] To simplify the model it is assumed that the magnetic field is a basic dipole aligned with and in the opposite direction of the rotation of Jupiter. The primary consequence of this simplification is a time-varying error in the magnetic field direction. The magnetic field strength is assumed to follow an inverse cube law $B = M/r_1^3$ where $M = 4.25 \times 10^{-4}$ Gauss $\cdot R_J^3$ and the plasma density is assumed constant at $N_e = 3 \times 10^9 \mathrm{m}^{-3}$.

Note from Equations (8) and (9) that the Lorentz force scales linearly with tether width but to the five-half power with tether length. If the force is known for a given tether orientation, position, and velocity, one can quickly recalculate the force for different tether sizes using this scaling property. Tether direction has a significant effect on the Lorentz force both in that the force is limited to be perpendicular to the tether and that the force magnitude depends on the dot product E_t. To reduce the scope of the problem tether orientation is assumed to be aligned with the position vector such that the tether is always pointing radially to or away from the center of mass of the primaries, unless stated otherwise. This results in the tether force being at near maximum and is also generally the stable tether attitude when not near moons.[20] Higher fidelity studies will consider the stability of the tether attitude while operating in proximity to smaller primaries.

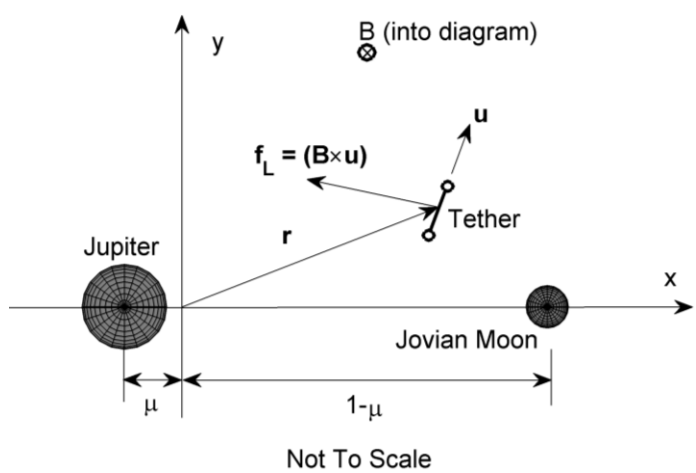

Figure 1. Planar diagram of CRTB frame including tether and Lorentz force directions

Figure 1gives an example diagram of the three-body frame centered at the system center of mass including the tether and the Lorentz forces. As described previously, the Lorentz force $\mathbf{f_L}$is perpendicular to both the tether orientation $\hat{\mathbf{u}}$ and the local magnetic field $\mathbf{B}$.

For all simulations in this study a set spacecraft mass of 1000 kg with a tether width of 0.01 m is used. The dynamics are considered at Io and Metis on a per-case basis to highlight differences deriving from changes in the magnetic field strength and relative plasma velocity.

EQUILIBRIUM POINTS

A primary interest is in tether modified equilibrium points within the three-body system. The initial method is a global approach of all possible equilibria in the *xy*-plane. The method grids over locations and calculates the unperturbed acceleration, then sets the tether orientation so the Lorentz force opposes this acceleration. The tether orientation to oppose the gravitational and centrifugal forces is calculated using a cross product:

$$\mathbf{u_{eq}} = \hat{\mathbf{z}} \times \ddot{\mathbf{r}} \tag{10}$$

$$\hat{\mathbf{u}}_{\mathbf{eq}} = \frac{\mathbf{u_{eq}}}{|\mathbf{u_{eq}}|} \tag{11}$$

Using a reference tether length L_0, this tether orientation is used to calculate the Lorentz force $\mathbf{f_{L_0}}$. The actual tether length required to produce sufficient force to counter the three-body acceleration $\ddot{\mathbf{r}}$ is found by taking advantage of the scaling properties of the Lorentz force:

$$L_{EQ}^{5/2} = \frac{|\ddot{\mathbf{r}}|}{|\mathbf{f_{L_0}}|} {L_0}^{5/2} \tag{12}$$

where L_{EQ} is the length of the tether required to generate a force that achieves equilibrium.

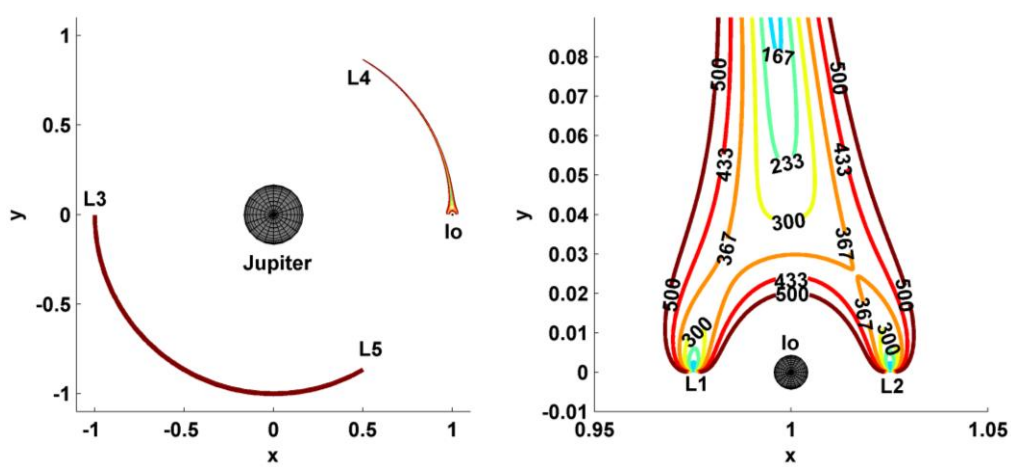

Figure 2. Contour levels representing locations of equilibrium points for varying tether lengths at Io.

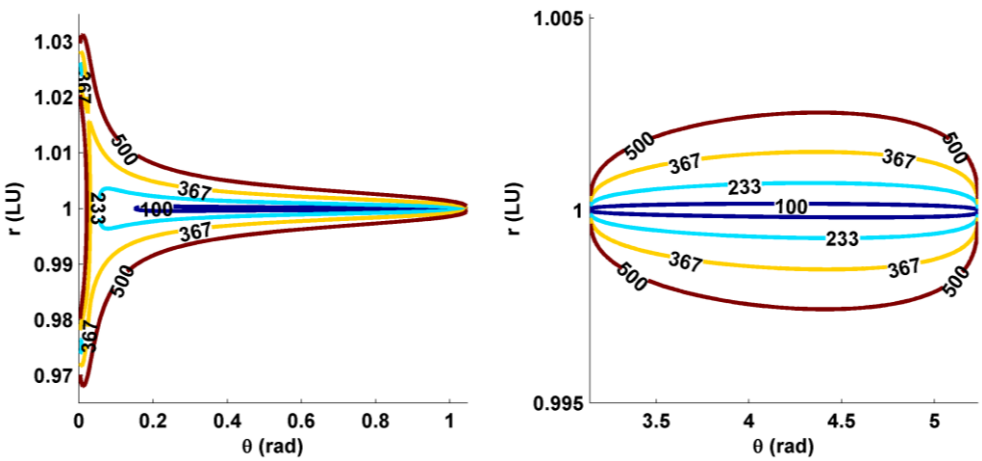

Figure 3. Curves of equilibrium points as a function of counter-clockwise angle from the line between primaries,θ, and distance from system center. Curves are between Io to L4 (left) and L3 to L5 (right)

Curves of equilibrium positions with constant tether length at Io are shown in Figure 2 and Figure 3. Intuitively, longer curves are associated with increased tether sizes. Figure 2 gives a global view of possible equilibrium points in the *xy*-plane of the rotating frame including a detailed view near Io. It can be seen that the curves only exist in the regions between the unperturbed L1/L2 and L4 points as well as the L3 and L5 points. Outside of these regions the tether orientation required to provide the correct force direction causes E_t in Equation (8) to be negative, hence no current is induced. Figure 3 further details these regions by plotting the curves in polar coordinates, highlighting that the curves close off at the Lagrange points. It can also be seen that the distance of the equilibrium points from system center remains near unity with the largest discrepancy occurring about L1 and L2.

This deviation is best examined in the detail plot in Figure 2. It is seen that tether lengths below 100 km do not have significant variations in equilibrium points about L1 and L2. As the length increases the contour curves expand about L1 and L2 until they connect with the curves originating from the L4 point at a length of approximately 370 km. This connection allows for a wide range of equilibrium points along the leading side of Io.

While the global approach gives good knowledge of what is possible to achieve in a general sense it lacks fidelity near the smaller primary, particular on the evolution of the location of the L1 and L2 points. An in-depth look at this evolution is made by using a continuation approach to get modified equilibrium points $L1^*$ and $L2^*$. The tether orientation is limited to the position vector-aligned attitude to reduce the problem scope. Using either Lagrange point as an initial guess along with an initially small tether size, a differential corrector is used to iterate on the spacecraft position until a perturbed equilibrium position is found. The tether length is then increased and the differential corrector rerun to get a new equilibrium point using the previous point as the new initial guess. The process is repeated until no new feasible equilibrium points exist.

The differential corrector uses derivatives of the total tether perturbed acceleration with respect to position. The z-based terms are included for completeness even though the equilibrium points are expected to be within the *xy*-plane. These derivatives are obtained using a numerical complex step approach. Complex step has the additional benefit of being less prone to machine precision error than finite difference methods.[21] The Newton update step is calculated using the following equation:

$$\boldsymbol{d}\mathbf{r}_{eq} = -\left(\frac{\partial \ddot{\mathbf{r}}_{EDT}}{\partial \mathbf{r}}\right)^{-1} \ddot{\mathbf{r}}_{EDT} \tag{13}$$

The update is iterated until the total acceleration magnitude is near zero within tolerance. Since the starting locations are the known L1 and L2 points with small steps in tether size, the initial guesses are sufficiently close for the simple differential corrector to converge.

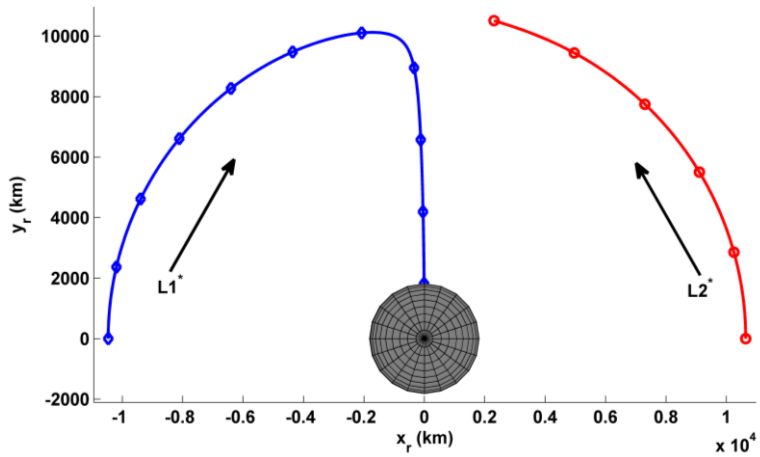

Figure 4. Lines of tether-perturbed L1* and L2* points at Io. Arrows indicate direction of evolution.

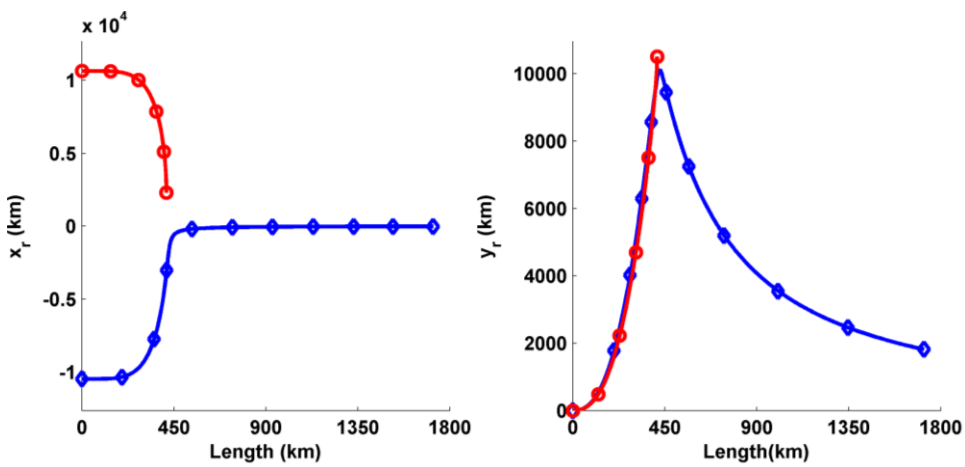

Figure 5. L1 (blue diamond) and L2 (red circle) equilibrium coordinates relative to Io as a function of tether length.

In Figure 4 the evolution of the equilibrium positions in the *xy*-plane centered at Io is plotted while Figure 5 shows the individual coordinate as a function of tether size. The notation $(*)_r$ is introduced to indicate position relative to Io. Recalling the start at the L1 and L2 points with $y_r = 0$ it is seen that as tether length is increased the equilibrium point shifts forwards. Further increases lead to curving towards the leading side of Io. At a length of 413 km the L2 point reaches conditions where the chosen tether orientation can no longer achieve an equilibrium point. The perturbed L1 points eventually shift towards the surface of Io and impact when tether length is 1718 km. This extreme length of tether is not practical but included for completeness. Note that the evolutions of these points is similar to results from Scheeres et al. in Reference 12 in that the points curve around the front of the primary and then down to the surface. Key differences are that those authors included tether attitude equilibrium rather than a general heuristic, and they developed the analysis in the Hill's model of motion, hence their results do not have a gap between the L1* and L2* curves.

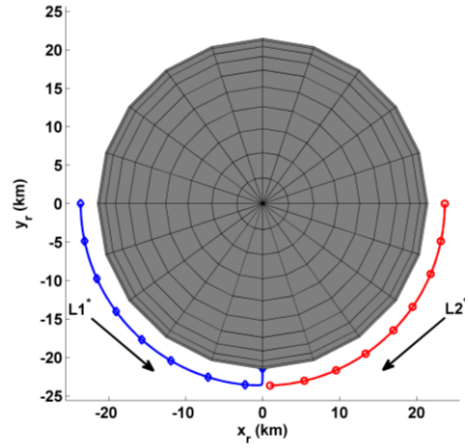

Figure 6. Lines of perturbed L1* and L2* points at Metis.

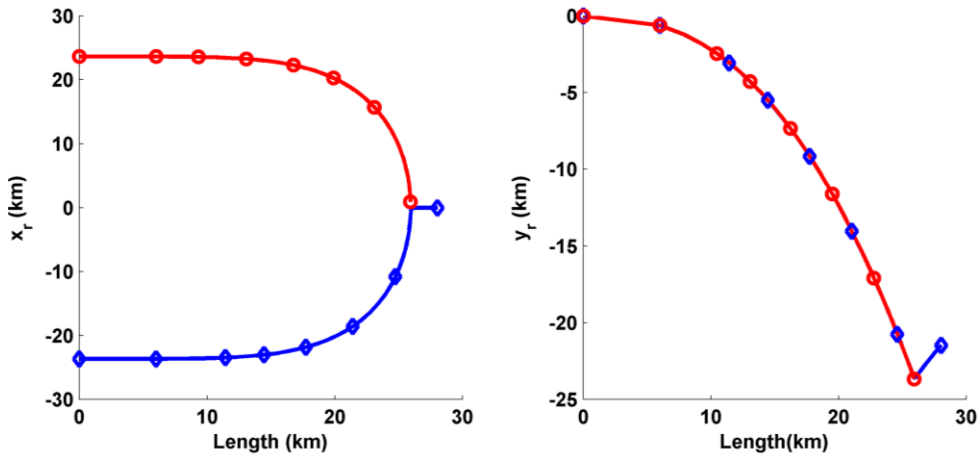

Figure 7. Metis L1 (blue diamond) and L2 (red circle) equilibrium coordinates as function of tether length.

In order to achieve more reasonable tether lengths the inner moonlet Metis is considered. The moonlet has a weaker gravity field and is in a stronger region of Jupiter's magnetic field. Plots are again made to show the equilibrium points, seen in Figure 6 and Figure 7. As Metis is only 1.83 R_j from Jupiter it's orbital velocity is greater than the rotating magnetic field; this switches the direction of the tether Lorentz force from that at Io causing the equilibrium points to shift towards the trailing edge of Metis. The weaker gravity and stronger Lorentz force allows for significantly shorter tether lengths with a 26 km tether capable of equilibrium directly trailing the moonlet. This difference in force magnitudes allows for unique possibilities including placing the spacecraft in a position where Metis itself functions as a partial radiation shield from Jupiter.[22] A major concern is that the average radius of the moonlet is only 21.5 km, meaning each tether end will be effectively on opposite sides of Metis. This gravity differential on the tether ends will lead to the tether collapsing and wrapping about the moonlet unless the width is increased to stiffen the tether. The fact that this small radius also results in a non-spherical gravity field is currently ignored.

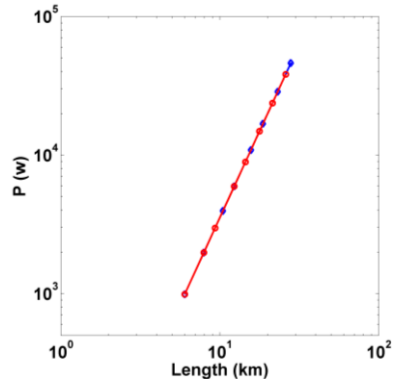

Figure 8. Ideal power generation at Metis is near-identical for L1* (blue) and L2* (red)

As a key benefit of electrodynamic tethers is power generation, the power derived from the tether at the modified equilibrium points is calculated for Metis. Since the equilibrium points include the tether force it is possible to indefinitely generate power without altering the orbit about Jupiter, assuming the equilibrium point can be maintained. The ideal power equation is a simple expression:

$$P = I \cdot L \cdot E_t \tag{14}$$

where the current I is given by (7). The power is plotted in Figure 8 where it is apparent that there is a near-linear relation with the logarithms of the variables. This relation is primarily due to the choice of tether orientation and relatively small variance in the spacecraft position resulting in a near constant current for all tether lengths. Additionally the power is nearly identical for both sets of equilibrium points, again a result of the relatively small difference in their positions. Basic substitution of Equations (7) and (8) into the power equation shows that power is proportional to $L^{5/2}$ and an analytical fit can readily be found as:

$$P \cong 11.220 L^{5/2} \tag{15}$$

where tether length is in kilometers and the power is in watts. A check of the relative error shows a maximum of 0.17% for the L1 points and 0.23% for L2 so the expression is reasonably accurate. For a tether of 25 km there is an ideal power of 35 kW, seven times the power capability of Juno's solar cells. To match Juno's upper limit of 500 W requires a tether length of only 4.6 km, clearly demonstrating the potential of tether-based power generation.

TETHER LYAPUNOV ORBITS

As an extension to equilibrium positions there is interest in the evolution of the L1 and L2 Lyapunov orbits due to tether forces from a radially aligned tether. Starting from known unperturbed orbits the Lorentz force is introduced and its effects on orbital shape, orientation, and stability are evaluated. The orbits are naturally characterized by both their integral of motion and the tether size. To limit the scope of the work only a limited range of these variables is considered by holding one constant while allowing the other to vary.

Conservative Approximation

The tether force is velocity dependent making the tether-perturbed problem non-conservative. As the energy change is path dependent it is unlikely that exact periodic orbits exist in general, although they have been found under special conditions in other non-conservative systems.[23] To transform the equations to a conservative system the assumption is made that the force magnitude is proportional to a constant

divided by the spacecraft in-plane distance from system center and the force direction is always perpendicular to the position vector:

$$\tilde{\mathbf{f}}_L = \frac{\alpha L^{5/2} w}{x^2 + y^2} (\hat{\mathbf{z}} \times \mathbf{r}) \tag{16}$$

where the constant α is determined by doing a least squares fit to the actual Lorentz force calculated over $0.95 < x^2 + y^2 < 1.05$ with zero spacecraft velocity relative to the rotating frame.

Table I. Lorentz force approximation parameters and comparative forces at bodies of interest.

Body	$\alpha\left(\mathrm{N} \cdot \mathrm{m}^{-7/2}\right)$	$\left\lvert\tilde{\mathbf{f}}_L\right\rvert_{r=1, L=25\ km}$ (N)
Europa	7.8179163e-012	0.0077
Io	4.6696398e-011	0.0461
Metis	-3.9632967e-009	3.9166

The parameter α is calculated at bodies of interest and shown in Table I. For Metis there is a negative value due to the body's velocity about Jupiter exceeding the rotational velocity of the magnetic field resulting in a drag-like force. A comparison of the approximated force magnitudes are also given for a tether length of 25 km. The decreasing distance from Jupiter results in differences of orders of magnitude between each body.

There are two main sources for inaccuracies in the approximation model force magnitude. As the line fit is imperfect the approximation breaks down as r deviates from near-unity. Additional error derives from the actual force dependency on the velocity of the tether relative to the magnetic field. The tether orientation is the same for both the full and approximate models resulting in zero error for the force direction. To quantify the approximation error calculations are made of the actual and approximate tether forces over a grid of radii and tangential velocities, v so at each grid point the spacecraft state is $\mathbf{X} = [r \quad 0 \quad 0 \quad 0 \quad v \quad 0]^T$.

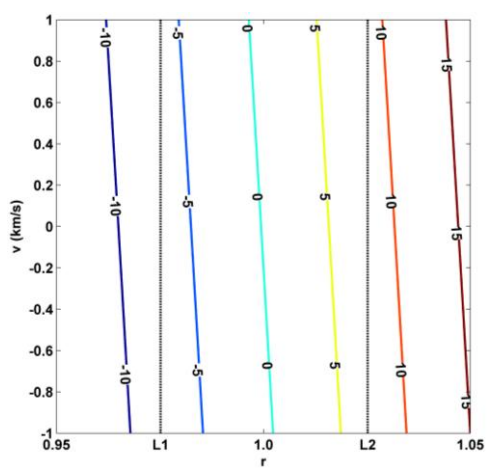

Figure 9. Relative error percentage in the force approximation at Io.

The analysis is applied at Io to get a relative error for the conservative force approximation, shown in Figure 9. Negative values indicate the actual tether force is larger than the conservative model approximation. Due to the size scaling of the force the relative error is independent of tether length. Looking at the figure it is clear that differing radii is the largest contributor to errors. The lack of precision in the fit leads to as high as 15% error while still relatively close to the moon's distance from Jupiter. Large periodic orbits can go beyond these radii although typical L1 and L2 orbits are expected to remain

within 15% error. At the unperturbed L1 and L2 points the error is at -7.11% and 7.94% respectively. These are roughly on order with expected errors introduced from assumptions made about the magnetic field strength and simple non-tilted dipole simplifications. The error is comparatively invariant to small changes in orbital velocity as the velocity relative to the plasma is on the order of tens to hundreds of kilometers per second.

The force approximation has an associated potential function:

$$V_L = \alpha L^{5/2} w \tan^{-1}\left(\frac{y}{x}\right) \tag{17}$$

The potential function allows for a new integral of motion by augmenting the standard CRTBP Jacobi constant:

$$C = 2(J + kV_L) - (u^2 + v^2 + w^2) \tag{18}$$

This integral of motion can be used to determine allowed regions of motion through zero velocity curves and provides a natural generating parameter for periodic orbit families.

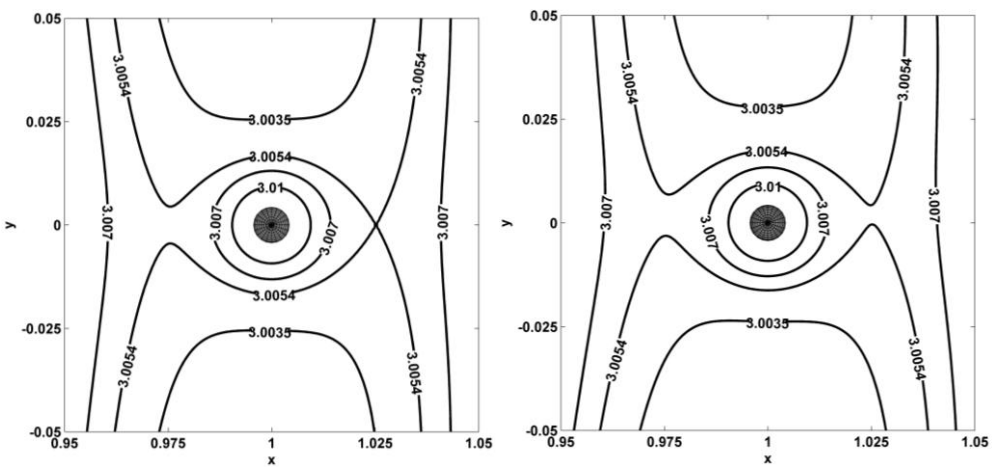

Figure 10. Detail view of tether (right) and non-tether (left) zero-velocity curves at Io.

Zero-velocity curves are used to visualize the general spacecraft dynamics. The values of these curves are found by setting the velocity in Equation (18) to zero and solving for the motion integral over a grid of locations. Plots of zero velocity curves for the unperturbed system, as well as with the new integral of motion at Io are given in Figure 10. The tether curves were made using a 150 km length tether to exaggerate effects.

The introduction of the tether leads to changes as the angle from the Jupiter-Io line varies. In the plots from Figure 10 it is seen that relative to the non-tether curve the contours of C = 3.0015 converge prograde of Io, increasing regions of motion, while they diverge retrograde resulting in shrinking regions of motion. As the Lorentz force is directed prograde about Io the spacecraft gains kinetic energy and travel becomes less restricted while traveling retrograde relative to Io reduces regions of motion. At C = 3.0054 the Hill's throats around L1 and L2 are seen which indicate that travel between Jupiter and Io is possible. Without tether forces these throats are nearly symmetric about and initially open at the x-axis. By introducing the tether forces it is seen that the throats are shifted slightly prograde, though with a 150 km tether the difference is limited. On the C = 3.0054 curve the throat is normally closed near L2 but it opens due to the tether force. Similar behavior is expected for the throat at L1.

Periodic Orbit Generation

Due to the existence of the tether force the equations of motion loses both xz-plane and x-axis symmetry, preventing the common approach of targeting perpendicular planar crossings to find periodic L1 and L2 orbits.[24] A full dimensioned targeting algorithm is implemented to search for periodic orbits.[25] In brief, the method starts with choosing a held position state (x_0, y_0, z_0) to enable checking for repeats of the initial state. Typical selections are crossings of the xy-, xz-, or yz-planes. As the final state is calculated at this crossing the plane crossing coordinate is automatically satisfied and can be ignored, leading to a reduced state vector $\boldsymbol{\xi}$. A constraint vector $\boldsymbol{K}$ is introduced to enforce that the trajectory returns to its initial state with an optional constraint to target specific energy levels, C:

$$\boldsymbol{K} = \begin{bmatrix} \boldsymbol{\xi_T} - \boldsymbol{\xi_0} \\ C - C^* \end{bmatrix}_{6\times 1} \tag{19}$$

Given an initial $\boldsymbol{\xi_0}$ that yields non-zero $\boldsymbol{K}$ calculate an update to the state $\Delta\boldsymbol{\xi_0}$ using a linear approximation:

$$\frac{\mathrm{d}\boldsymbol{K}}{\mathrm{d}\boldsymbol{\xi_0}} \Delta\boldsymbol{\xi_0} = -\boldsymbol{K} \tag{20}$$

$$\frac{\mathrm{d}\boldsymbol{K}}{\mathrm{d}\boldsymbol{\xi_0}} = \begin{bmatrix} \mathrm{d}\boldsymbol{\xi_T}/\mathrm{d}\boldsymbol{\xi_0} - \mathbf{I}_{5\times 5} \\ \mathrm{d}C/\mathrm{d}\boldsymbol{\xi_0} \end{bmatrix}_{6\times 5} \tag{21}$$

$$\frac{\mathrm{d}\boldsymbol{\xi_T}}{\mathrm{d}\boldsymbol{\xi_0}} = \frac{\partial\boldsymbol{\xi_T}}{\partial\boldsymbol{\xi_0}} + \frac{\partial\boldsymbol{\xi_T}}{\partial T}\frac{\partial T}{\partial\boldsymbol{\xi_0}} \tag{22}$$

Details of the corrector equations used are derived in Reference 25. An important attribute of the algorithm is its use of singular value decomposition (SVD) to approximate matrix inverses, allowing it to easily handle over or under constrained problems as well as singularities.

The algorithm is used iteratively to generate families of orbits characterized by either tether length of the motion integral. The initial states of these orbits are modified from those found in the corrector algorithm such that they more closely resemble the perpendicular x-axis crossings characteristic of standard three-body periodic orbits. Starting from the first member of each family these new initial states are found by propagating each orbit and finding locations where $u_0 = 0$. As each orbit is a closed loop there is always a minimum of two such locations. Out of the found candidate locations the new initial state is chosen closest proximity to the state of the preceding orbit within the family. Each orbit of the family is then characterized by their initial state, periodic time, and tether length. A stability analysis is applied to every orbit in both families and the stability indices are parameterized by the size of the tether.

To obtain $\partial\boldsymbol{\xi_T}/\partial\boldsymbol{\xi_0}$ the convenient and accurate numerical complex step method is again used. For each periodic orbit the state transition matrix over one period, also known as the Monodromy matrix, is calculated. The eigenvalues of this matrix indicate the stability of the periodic orbit. These eigenvalues are used to calculate stability indices using Equation (**23**). As the eigenvalues occur in reciprocal pairs only three unique stability indices exist. Additionally, because the system is autonomous one index is trivial as it is always 2, representing a perturbation along the orbit trajectory.[23] For linear stability the remaining two indices must be real and have magnitudes less than 2 otherwise the orbit is unstable with larger magnitudes representing more unstable orbits.

$$b_i = \lambda_i + 1/\lambda_i \tag{23}$$

For planar periodic orbits the stability indices are denoted as vertical or horizontal, b_v and b_h respectively. The horizontal indices correspond to perturbations within the orbit plane while the vertical indices are out-of-plane deviations.[26]

Variable Length Families

First there is an analysis of the effects of varying tether size at constant C on the L1 and L2 Lyapunov orbits at Io. Metis is not considered due to the close proximity of the equilibrium points to the surface. For both L1 and L2 a representative starting orbit is selected from the non-tether perturbed Lyapunov families. The only criteria used for initial selection is a general consideration of the approach distance to Io. The initial L1 orbit has $C = 3.0025008$ with a period of 3.5872 TU (24.24 hr) while the L2 orbit is at $C = 3.0024488$ with period 3.6613 (24.74 hr). Each initial orbit is then extended into a family of orbits by increasing tether length and using the differential corrector to return to a periodic orbit while keeping the integral of motion constant. As will be seen, reflections occur where the tether length switches between increasing and decreasing to continue the family. At these reflections the continuation method temporarily varies x instead of length to generate initial guesses for the next member of the family. The L2 family ends with impacting the surface of Io, while the L1 family is continued until convergence becomes difficult without using unreasonably small steps. The reasoning for this is discussed below.

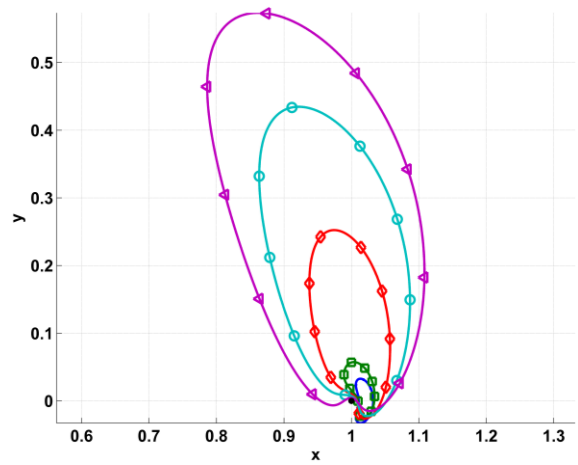

Figure 11. Evolution of L1 Lyapunov orbits at constant C.

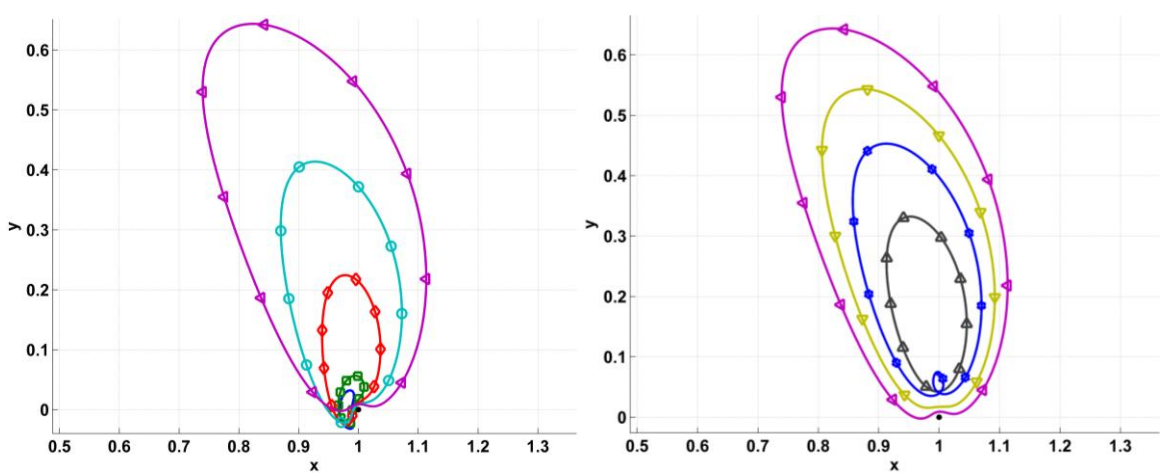

Figure 12. Evolution of L1 orbits from no tether up to maximum orbit distance (left) and after maximum distance (right)

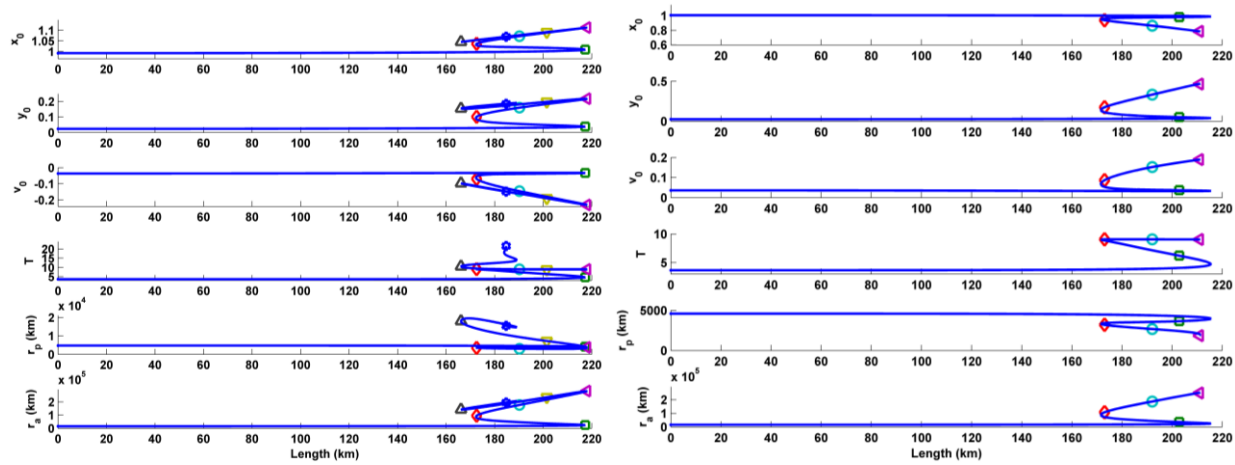

Figure 13. Characteristic curves of L1 and L2 families, including "apses".

Figure 11 plots a few of the orbits from the L2 family including the initial unperturbed orbit and the final orbit before impact. Due to the choice of different energy levels between the families the L1 family does not impact Io and has additional orbits in the family. The L1 orbits are plotted in Figure 12 where two plots are used for clarity. The left plot shows orbits until the family achieves its maximum distance from Io while the orbits after this point are shown in the right plot. Figure 13 gives the characteristic curves for both families, with markers correlating to the orbits plotted in the trajectory figures.

Starting with a qualitative analysis of the orbits, for both the L1 and L2 families increasing tether length causes the orbits to shift forward and slightly rotate about Io. It is clear that the orbits are not symmetric about the x-axis as there is bulging on the leading side of the moon due to the positive y-direction of the Lorentz force. For small orbits that remain within a few Io radii of the moon the L1 and L2 families are near-reflections about Io. With larger orbits the trajectories of both families tend to follow the curve of Io's orbit about Jupiter as they effectively depart from and re-encounter Io at non-resonant intervals. The last orbit found in the L1 family (denoted with blue hexagon markers) is particularly dynamically interesting in that half of its orbit time (~88 hr) is spent in a loop with a smaller inner loop near its closest approach. Distances from Io during this looping time range from a "periapse" of 15470 km to 31630 km.

Looking at the characteristic curves given in Figure 13 shows that the families are initially near-invariant to changes in tether length. It is only after lengths exceeding 100 km that notable differences occur, however these changes are small relative to the variations that start after the first reflection at 217 km tether length. The L2 curves go through a second reflection before impacting while the L1 curves go through seven reflections before the corrector encounters convergence difficulties. Each reflection occurs at smaller changes in tether length which can be seen clearest in the plot of L1 orbital period. The change in tether length between the last two reflections is only 1 km. It is this shrinking reflection interval that leads to difficulty in converging to new periodic orbits as the step sizes to enable convergence become infeasibly small. Additionally the orbit itself becomes effectively invariant with the only notable difference as slowing growth in the small looping regions mentioned earlier.

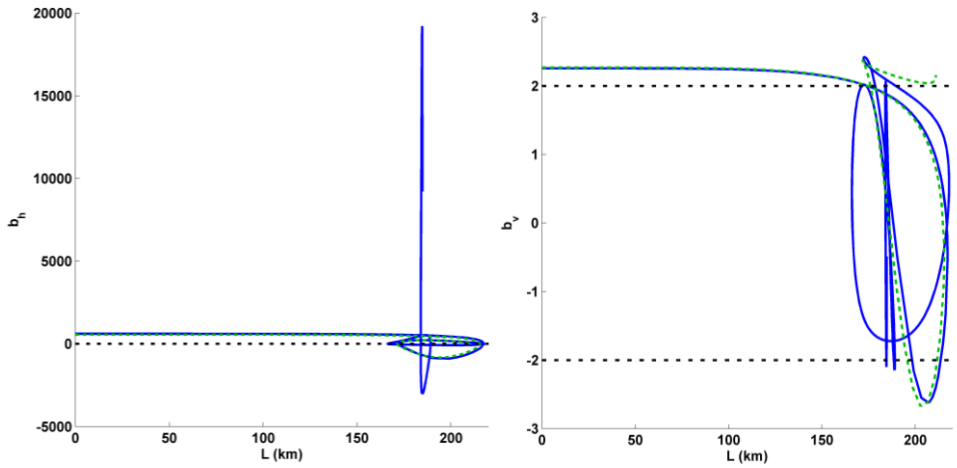

Figure 14. Horizontal (left) and vertical (right) stability indices for the L1 (solid) and L2 (dash) Lyapunov families at constant C. Lines of critical value included for reference.

Consider the stability indices given by Figure 14, where the indices have been separated by the vertical and horizontal grouping. Both indices are typically real valued, and instances where imaginary components appear are random and on the order of 10^{-14}. These imaginary values are attributed to numerical error involved with the complex step derivative method used. Comparing the two families it is seen that both indices tend to follow the same general shape although the quantitative differences increase through the family continuation. The effect is most noticeable after the second reflection where the L2 vertical indices diverge from the L1 line as the L2 orbits approach and ultimately impact Io.

As was seen in the characteristic curves the tether length initially has little effect on the indices before the 100 km tether length. With each successive reflection the indices become increasingly sensitive to changes in tether length to the point that they appear to be vertical lines. The indices for out of plane perturbations consistently remain within or just beyond stability. Horizontal stability is atypical and usually occurs during a reflection where the indices are rapidly changing from positive to negative values. As mentioned, orbits where the magnitudes of both the vertical and horizontal indices are less than the critical value of two are dynamically stable. Due to the sensitivity of the indices to changes in tether length after several reflections it becomes difficult to precisely find stable orbits, however they do exist. Examples of the stable orbits that occur during the first reflection for the L1 and L2 families can be seen in Figure 11 and Figure 12. These are the second smallest orbits plotted and are indicated by the green square makers. The orbits occur with a tether length of approximately 215 km and closely resemble perturbed versions of the originating zero-length tether orbits. No more stable orbits exist for the L2 family. The L1 family has limited number of additional stable orbits. One other stable orbit was successfully identified and is included in the right plot of Figure 12, marked with upward pointing triangles. The orbit leads Io in a simple ellipse-like shape far from the Jovian moon with a closest approach of 18000 km from moon center. The stability of the discussed orbits is verified by propagating over 100 orbital periods with no notable departures.

Varying the Integral of Motion

Allowing for different values for the integral of motion is needed for a full analysis of tether-perturbed periodic orbits. To keep the scope manageable an in-depth analysis is considered at two constant tether lengths for both L1 and L2 families. The first case uses a 150 km tether while the second is at 200 km. While orbits at lower lengths were considered they do not sufficiently differ from either the 150 km or zero-length orbits to be dynamically interesting.

Starting from a small orbit about the tether-modified equilibrium point, iterative changes to the motion integral described by Equation (18) are made and the state is converged to a new orbit using the

differential corrector. Once two orbits have been found a basic linear extrapolator is used to guess the next state to speed convergence. The orbits are continued until they impact Io or undergo rapid reflections such that practical convergence becomes difficult with reasonable step sizes.

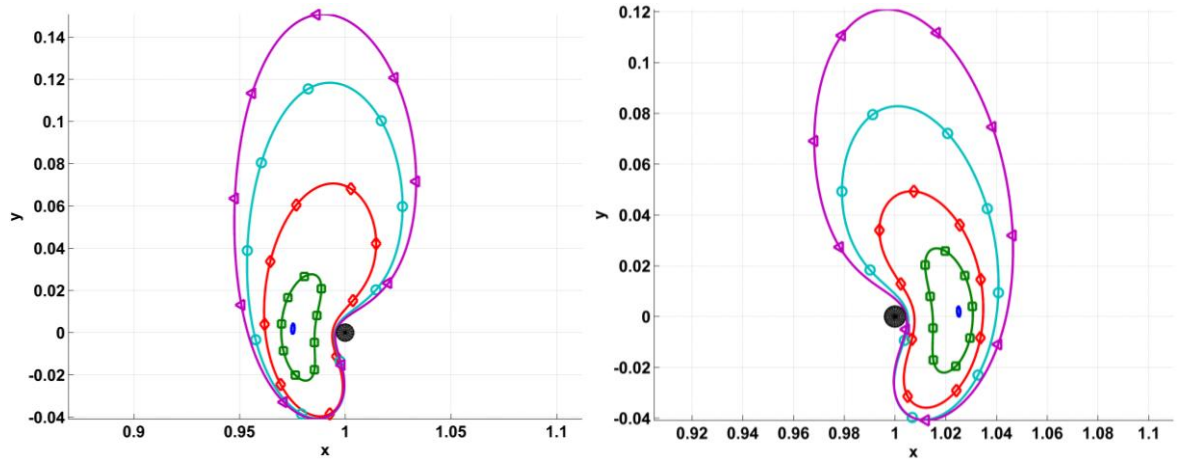

Figure 15. Example L1 (left) and L2 (right) Lyapunov orbits at constant tether length of 150 km.

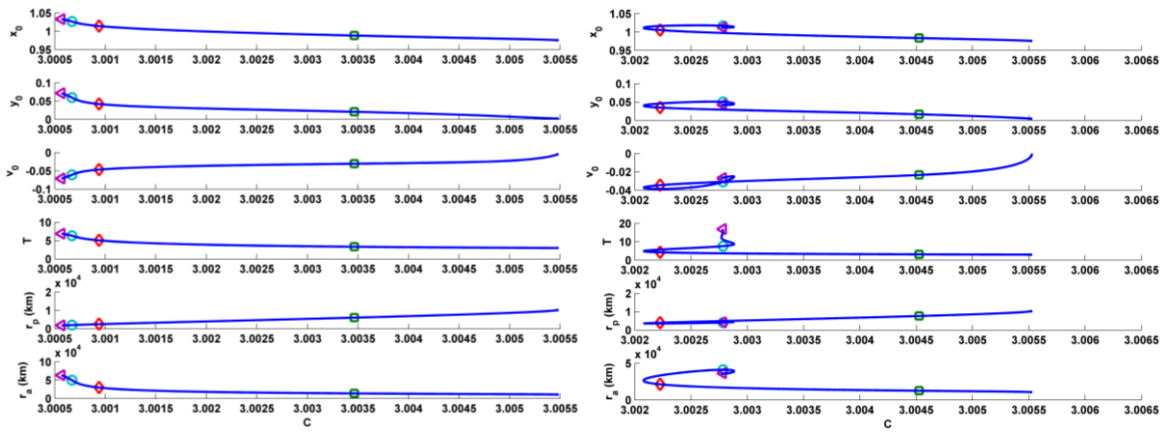

Figure 16. Characteristic curves for L1 (left) and L2 (right) families as motion integral varies with constant tether length.

Several orbits from both the L1 and L2 families are given in Figure 15 while Figure 16 plots the characteristic curves. As expected the families start as small orbits about the equilibrium points which have been shifted towards the leading side of Io due to tether forces. These initial orbits are at the maximum motion integrals of 3.0054928 and 3.0054301 for L1 and L2 respectively. The orbit size increases as C is decreased, with initial orbits closely resembling typical Lyapunov orbits. At the end of the families the orbits exhibit bulging on the leading side of Io. The sensitivities of the families to changes in the motion integral increase as the families are continued with most of the changes occurring over a small sub-interval of the total range of motion integral considered. While this is indicative of an upcoming reflection both families impact Io and are considered complete for the purposes of this paper.

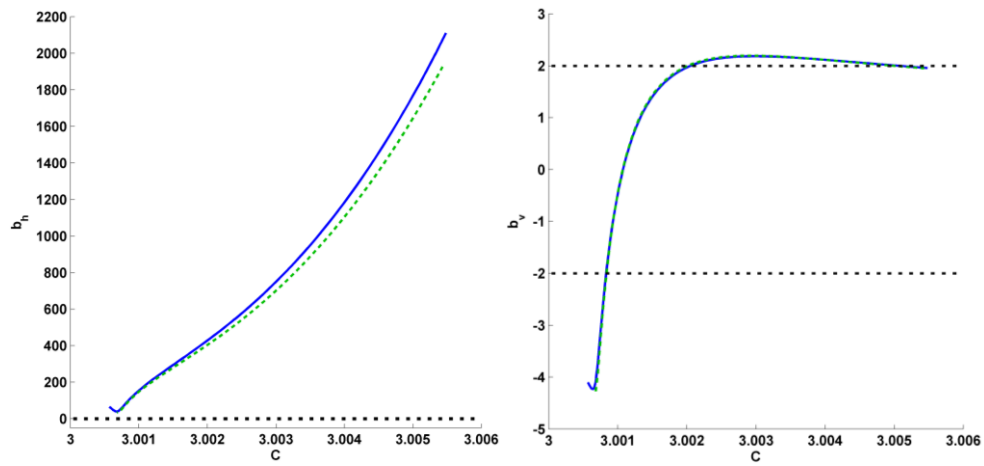

Figure 17. Horizontal and vertical stability for L1 (solid) and L2 (dash) families with 150 km tether length.

The stability indices of the families using a constant tether length of 150 km are shown in Figure 17. The imaginary components of the indices are again negligently small and are ignored. Note that the curves for the vertical indices are near-identical making differentiation difficult. The horizontal indices have a minimum value of 34, above the critical value indicating that no orbits within the families are fully stable. Vertical stability alternates through the families with a total of three crossings of the critical value. These crossings indicate that there are at least two simple and one period-doubling bifurcations of the periodic orbit that can be followed in later work to generate additional periodic orbit families.

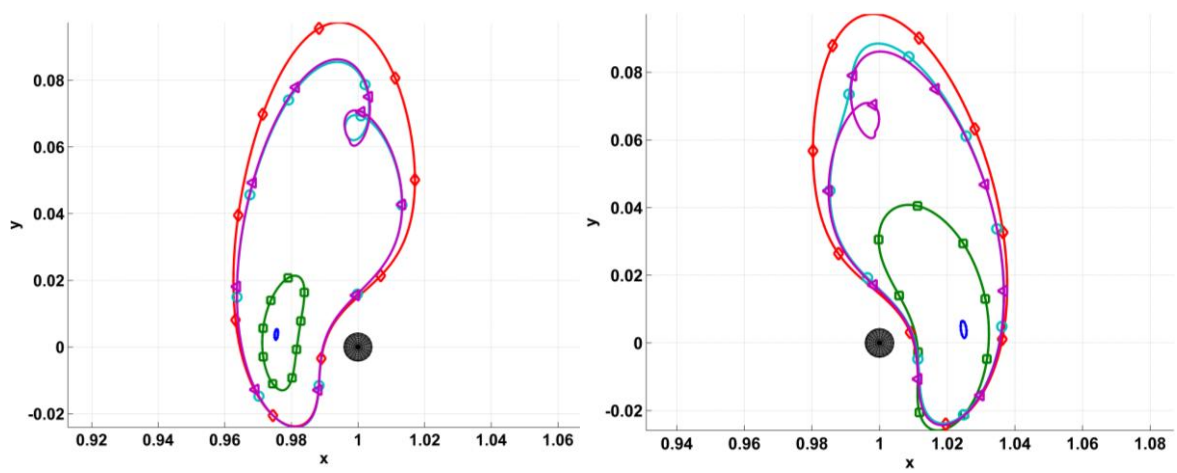

Figure 18. Tether-forced Lyapunov periodic orbits at constant tether length of 200 km.

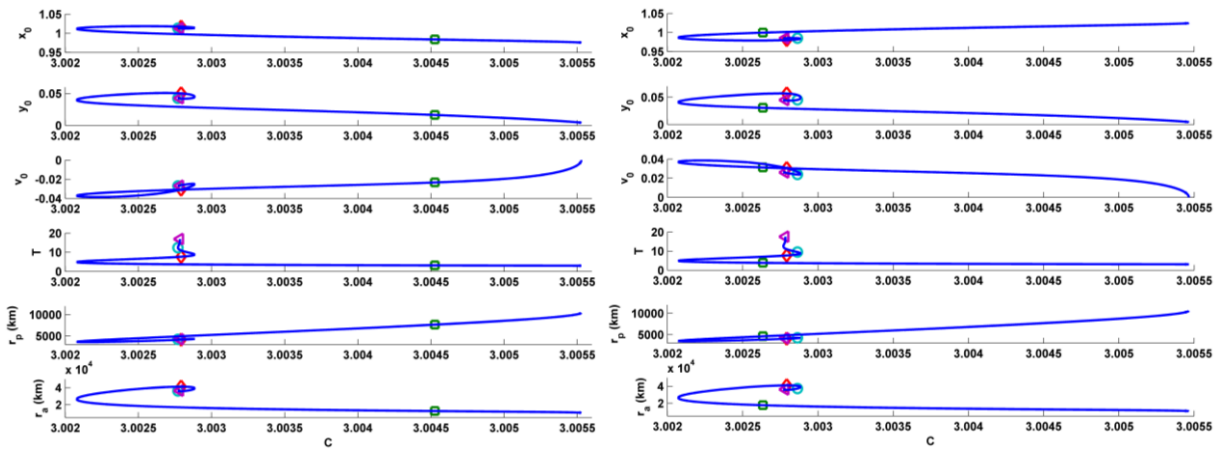

Figure 19. Non-zero initial states, periodic time, and "apse" distance for L1 and L2 families as motion integral varies.

The L1 and L2 families calculated using a constant 200 km length tether are given in Figure 18. Neither family experiences an impact with Io resulting in the continuation process ending after a series of increasingly frequent reflections similar to the orbital families where length was allowed to vary. The orbits found before the first reflection are qualitatively similar to those found at the 150 km length. Beyond the first reflection the orbits continue to grow in size up to a maximum as can be seen from the sub-plot of "apoapse" given in Figure 19. As the families continue the orbits reduce in size before developing fractal-like looping dynamics similar to what was observed for the constant motion integral families. All the characteristic curves additionally have fractal-like spiraling over successive reflections with the exception of periodic time which monotonically increases.

The orbits shown from the L1 family highlight the small orbit about the tether modified equilibrium point, the orbit with maximum Io distance (diamond markers), the last orbit found in the family (triangles), as well as two stable orbits(squares and circles). As the L2 family is a near-reflection of the L1 family it does not include the stable orbits but instead plots an orbit with similarities to a rotated and shifted standard Lyapunov orbit (squares) Two of the orbits (marked by circles and triangles) in the L2 family are shown specifically to highlight that changes to orbital shape become predominantly limited to the looping structure.

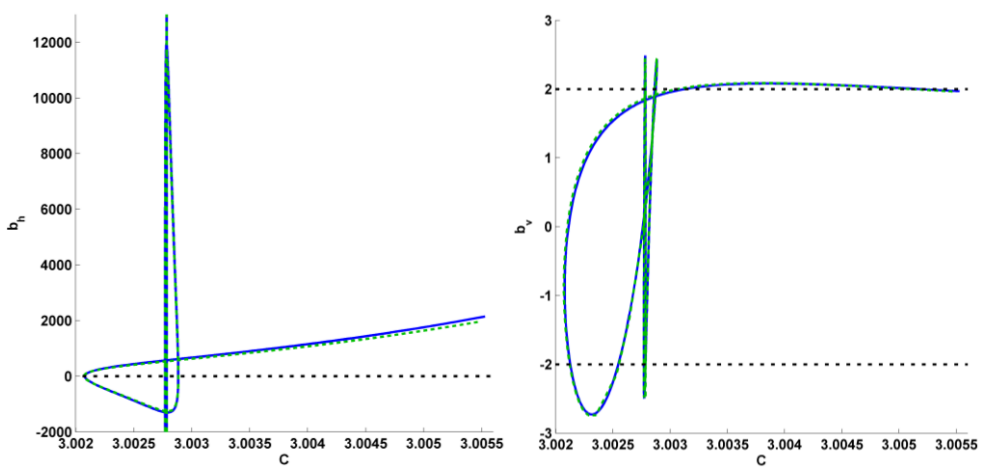

Figure 20. Varying stability indices for L1 (left) and L2 (orbits) with constant tether length of 200 km.

The stability indices are given in Figure 20 where again there are no significant imaginary components. Note that for improved visibility the horizontal indices plot has been cropped to exclude significant spikes

of -92000 and 376000 that occur over the final two reflections of the families. It is clear that both vertical and horizontal indices go through the stable region indicating the existence of stable orbits. As was seen for the variable length families the horizontal indices are highly sensitive to changes to C during these stability transitions, to the point that db_h/dC becomes on the order of 10^{13}. This sensitivity makes finding orbits within the relatively small stability region numerically challenging, and they are unlikely to be caught naturally in an automated continuation algorithm.

CONCLUSIONS

The introduction of electrodynamic tethers to the CRTB problem leads to changes in both the equilibrium points and the periodic orbits of the model. As discussed previously one of the main benefits of utilizing a tether is to enable a self-powered spacecraft in a stationary observing location relative to a minor body. At Metis the power required for current spacecraft can be generated with a tether only 4 km long. While the power production decreases with distance from Jupiter the tether is still capable of providing more than 400 W of power with a tether length of 20 km. Historic data from the tether test satellite SEDS shows a 20 km tether having a mass of 7 kg, translating to 1.4 kg for the 4 km tether.[27] This has mass advantages over the alternatives of larger solar arrays or RTGs which are typically on the order of tens of kilograms. Considering that the power generated scales exponentially with tether length longer tethers actually become more efficient in terms of power produced per tether mass.

In addition to the power generation, these modified equilibrium points provide opportunities for new mission designs. If there is interest in placing the spacecraft in an equilibrium point for constant observation geometries of a moon, mission planners are no longer limited to choosing one of a few points. Assuming a degree of controllability in tether length it would be possible to transfer across a range of equilibrium points for long-term constant observation. Selection criteria for these locations can include utilizing the bodies as partial shielding from Jovian radiation. A more innovative concept is the use of a probe at the end of the tether to physically sample the moons while the Lorentz force holds the spacecraft in a steady location, obviously this concept assumes highly precise control of the tether.

A problem with using the equilibrium points near the moons is that the points are generally unstable.[14] An alternative to maintaining a highly-constrained position is using periodic orbits about equilibrium points. After generating multiple families of basic Lyapunov orbits it is found that stable orbits do exist for differing tether lengths and energy levels. Investigations of more advanced orbits via bifurcations will likely find more stable orbits of interest. This has significant implications from a mission design standpoint. At the most basic level these orbits can be used as long-term parking orbits near a moon without requiring corrective maneuvers. Additionally power can be generated over the course of the orbit without the need to maintain position as would occur at equilibrium points. Assuming the orbit is favorable for science data it can be captured into for significantly less cost than typical low-altitude science orbits deep in the moon's gravity well.

REFERENCES

[1] Nybakken, Rick, "The Juno Mission to Jupiter, a Pre-Launch Update." Aerospace Conference, 2011 IEEE, pp. 1-8, DOI: 10.1109/AERO.2011.5747272

[2] Sanmartín, J. R., Martínez-Sánchez, M., and Ahedo, E., "Bare Wire Anodes for Electrodynamic Tethers," Journal of Propulsion and Power, Vol. 9, No. 3, 1993, pp. 353–360.

[3] Samanta Roy, R. I., Hastings, D. E., and Ahedo, E., "Systems Analysis of Electrodynamic Tethers," Journal of Spacecraft and Rockets,Vol. 29, 1992, pp. 415–424.

[4] Bombardelli, C., Lorenzini, E.C., Curreli, D., Sanjurjo-Rivo, M., Lucas, F.R., Peláez, J., Scheeres, D.J., Lara, M. "Io Exploration with Electrodynamic Tethers," AIAA/AAS Astrodynamics Specialist Conference and Exhibit, Honolulu, Hawaii, 18-21 Aug. 2008

[5]Sanmartin, J.R., Charro, M., Lorenzini, E.C., Garrett, H.B., Bombardelli, C., Bramanti, C. "Electrodynamic Tether at Jupiter-II: Fast Moon Tour After Capture," IEEE Transactions on Plasma Science, Vol. 37, No. 4.,April 2009, pp. 620-626

[6]Bombardelli, C., Lorenzini, E.C., and Sanmartín, J.R., "Jupiter Power Generation with Electrodynamic Tethers at Constant Orbital Energy", Journal of Propulsion and Power, Vol. 25, No. 2, 2009, pp. 415-423.

[7]Gabriel, S.B., Jones, R.M., and Garrett, H.B., "Alfven Propulsion at Jupiter", Intl. Conference on Space Tethers for Science in the Space Station Era, Venice, Italy, Oct. 4-8, 1987

[8]Sanmartín, J.R. and Lorenzini, E.C., "Exploration of Outer Planets Using Tethers for Power and Propulsion," Journal of Propulsion and Power, Vol. 21, No. 3, May-June 2005, pp. 573-576

[9]Sanmartin, J.R., Charro, M., Lorenzini, E.C., Garrett, H.B., Bombardelli, C., Bramanti, C. "Electrodynamic Tether at Jupiter-I:Capture Operations and Contraints," IEEE Transactions on Plasma Science, Vol. 36, No. 5., Oct. 2008, pp. 2450-2458

[10]Tragesser, Steven G. and San, Hakan, "Orbital Maneuvering with Electrodynamic Tethers", Journal of Guidance, Control, and Dynamics, Vol.26, No. 5, Sept.-Oct. 2003, pp. 805-810.

[11]Sanmartin, J.R., Estes, R.D., Lorenzini, E.C., and Elaskar, S.A., "Efficiency of Electrodynamic Tether Thrusters," Journal of Spacecraft and Rockets, Vol. 43, No. 3, May-June 2006, pp. 659-666

[12]Peláez, J., Bombardelli, C., and Scheeres, D.J. , "Dynamics of a Tethered Observatory at Jupiter," Journal of Guidance, Control, and Dynamics, Vol. 35, No. 1, Jan.-Feb. 2012, pp. 195-207

[13]Zanutto, D., Curreli, D., and Lorenzini, E.C., "Stability of Electrodynamic Tethers in a Three-Body System," Journal of Guidance, Control, and Dynamics, Vol. 34, No. 5, Sept.-Oct. 2011, pp.1441-1456

[14]Bombardelli, C. and Peláez, J., "On the Stability of Artificial Equilibrium Points in the Circular Restricted Three-body Problem," Celest Mech Dyn Astr, 2011, pp.13-26

[15]Pelaez, J. and Lara, M., "Dynamics of Fast-rotating Tethered Satellites," Monografias de la Real Academia de Ciencias de Zaragoza 32, 2009, pp. 75-83

[16]Lam, T. and Whiffen, G.J., "Exploration of Distant Retrograde Orbits around Europa," 15th AAS/AIAA Space Flight Mechanics Meeting, Copper Mountain, CO, January 23-27, 2005

[17]Russell, R.P. and Brinckerhoff, A.T., "Circulating Eccentric Orbits around Planetary Moons," Journal of Guidance, Control, and Dynamics, Vol. 32, No. 2, March-April 2009, pp. 423-435

[18]Lantoine, G. and Russell, R.P., "Near Ballistic Halo-to-Halo Transfers between Planetary Moons," The Journal of the Astronautical Sciences, July 2011, Vol. 58, Issue 3, pp. 335-363

[19] Divine, N. and Garrett, H.B., "Charged Particle Distributions in Jupiter's Magnetosphere," Journal of Geophysical Research, 1983, Vol. 88, pp. 6889 - 6903

[20]Robinson, W.J., "The Restricted Problem of Three Bodies with Rigid Dumb-bell Satellite," Celestial Mechanics, Vol. 8, No. 2, 1973, pp. 323–330.

[21]Martins, J.R.R.A, Sturdza, P., and Alonso, J.J., "The Complex-step Derivative Approximation." ACM Transactions on Mathematical Software, Vol. 29, Iss. 3, Sept. 2003, pp. 245-262

[22]Hess, W.N., Birmingham, T.J., and Mead, G.D., "Absorption of Trapped Particles by Jupiter's Moons." Journal of Geophysical Research, Vol. 79, No. 19, July 1,1974

[23]Broucke, R., "Stability of Periodic Orbits in the Elliptic, Restricted Three-body Problem." AIAA Journal, Vol. 7, No. 6, June 1969

[24]Russell, Ryan. "Global Search for Planar and Three-Dimensional Periodic Orbits Near Europa." The Journal of Astronautical Sciences, Vol. 54, No. 2, 2006, pp. 199-226.

[25]Russell, Ryan P. and Martin, Lara. "Long-Lifetime Lunar Repeat Ground Track Orbits." Journal of Guidance, Control, and Dynamics, Vol. 30, No. 4, July-Aug. 2007, pp. 982-993

[26] Hénon, M., "Vertical Stability of Periodic Orbits in the Restricted Problem. II: Hill's case," Astronomy and Astrophysics, Vol. 30, No. 2, 1974, pp. 317–321.

[27]Lorenzini, E.C., Bortolami, E.B., Rupp, C.C, and Angrilli F., "Control and Flight Performance of Tethered Satellite Small Expendable Deployment System-II." Journal of Guidance, Control, and Dynamics. Vol. 19, No. 5, Sept.-Oct. 1996, pp. 1148-1156